Suppressing effect of Ca^{2+} blips on puff amplitudes by inhibiting channels to prevent recovery

Yuan Chen,[1] Hong Qi,[2] Xiang Li,[1] Meichun Cai,[1] Xingqiang Chen,[1] Wen Liu,[1] and Jianwei Shuai[1,3,*]

[1]*Department of Physics, College of Physics Science and Technology, Xiamen University, Xiamen 361005, China*

[2]*Complex Systems Research Center, Shanxi University, Taiyuan 030006, China*

[3]*State Key Laboratory of Cellular Stress Biology, Innovation Center for Cell Signaling Network, Xiamen University, Xiamen 361102, China*

(Received 17 April 2016; published 15 August 2016)

As local signals, calcium puffs arise from the concerted opening of a few nearby inositol 1,4,5-trisphospate receptor channels to release Ca^{2+} ions from the endoplasmic reticulum. Although Ca^{2+} puffs have been well studied, little is known about the modulation of cytosolic basal Ca^{2+} concentration ($[Ca^{2+}]_{Basal}$) on puff dynamics. In this paper we consider a puff model to study how the statistical properties of puffs are modulated by $[Ca^{2+}]_{Basal}$. The puff frequency and lifetime trivially increase with the increasing $[Ca^{2+}]_{Basal}$, but an unexpected result is that the puff amplitude and the maximum open-channel number of the puff show decreasing relationship with the increasing $[Ca^{2+}]_{Basal}$. The underlying dynamics is related not only to the increasing puff frequency which gives a shorter recovery time, but also to the increasing frequency of blips with only one channel open. We indicate that Ca^{2+} blips cause the channels to be inhibited and prevent their recovery during interpuff intervals, resulting in the suppressing effect on puff amplitudes. With increasing $[Ca^{2+}]_{Basal}$, more blips occur to cause more channels to be inhibited, leaving fewer channels available for puff events. This study shows that the blips may play relevant functions in global Ca^{2+} waves through modulating puff dynamics.

DOI: 10.1103/PhysRevE.94.022411

I. INTRODUCTION

As a second messenger of cells, calcium ion (Ca^{2+}) acts as an important signal to regulate various cellular processes, such as gene expression, muscle contraction, metabolism, and memory [1,2]. At the resting state, the free cytosolic Ca^{2+} concentration ($[Ca^{2+}]$) is maintained at a few tens of nM [1,3]. Most of the Ca^{2+} ions in cells are stored in the endoplasmic reticulum (ER) in which $[Ca^{2+}]$ can be $300\,\mu M$ or even above $2mM$ [4,5]. When inositol 1,4,5-trisphosphate (IP_3) messengers are generated upon responding to extracellular stimulus and bind to IP_3 receptors (IP_3R) on ER, the IP_3R channels become open to release Ca^{2+} ions into the cytosol from the ER. The oscillating $[Ca^{2+}]$ performs its physiological functions.

Whether the IP_3R channel is open or not is determined by the binding and unbinding of IP_3 and Ca^{2+} to the channel. The binding of IP_3 always promotes the open probability of IP_3Rs, while the Ca^{2+} binding shows a biphasic dynamics, because there are activating and inhibiting Ca^{2+} binding sites on IP_3Rs. The low cytosolic $[Ca^{2+}]$ can typically activate the channels and increase the open probability of IP_3Rs, giving the process of the Ca^{2+}-induced Ca^{2+} release (CICR). However, when the cytosolic $[Ca^{2+}]$ is larger than several μM, the Ca^{2+} ions will typically bind on the inhibiting sites of channels, which closes the channels [6,7].

It has been suggested that the IP_3R channels are distributed in clusters on the ER to generate different Ca^{2+} signals [8]. The fundamental signal is a blip which is a random opening of individual IP_3Rs [9,10]. The open channel gives a sudden rise of nearby $[Ca^{2+}]$ which can propagate to activate the neighboring IP_3Rs within a cluster, generating puffs with several open channels. Furthermore, the spreading $[Ca^{2+}]$ in cytosol can induce more channels to open in adjacent clusters via the CICR mechanism, resulting in the generation of global waves [11]. Therefore, the puffs play an important role in the calcium signals as an essential process to form global waves [12].

Experimentally, it has been shown that the basal $[Ca^{2+}]$ ($[Ca^{2+}]_{Basal}$) accumulates slowly resulting from puff activities during a long interwave period [11]. Ca^{2+} puffs occur at increasing frequency throughout the interwave interval because of the recovery of channels from their refractory state. The increasing puffs generate the liberated $[Ca^{2+}]_{Basal}$. When the amount of $[Ca^{2+}]_{Basal}$ liberated by puffs becomes sufficient, the next wave is initiated. As a result, Ca^{2+} puffs play a crucial role in generating repetitive Ca^{2+} global oscillations [11].

The dynamics of the Ca^{2+} puffs has been studied extensively not only in experiments [13–15], but also with theoretical models [16–18]. Computational models provide valuable insights into the Ca^{2+} signaling mechanisms. Some models focused on the transition dynamics from blips to puffs [19] and some on the dynamics from puffs to waves [20]. It has been suggested that the puff is terminated by self-inhibition [17]. For puffs, it is important to know how different factors, such as $[IP_3]$, Ca^{2+} buffers, and the cluster size, affect the puff dynamics in amplitude, lifetime, and frequency [18,21]. Rüdiger *et al.* [22] indicated that immobile buffers affect $[Ca^{2+}]$ transient levels only, while mobile buffers in general reduce both transient and stationary levels of $[Ca^{2+}]$ around IP_3R clusters. Cao *et al.* [18] found that the mean puff amplitude has a linear relation with cluster size N at small N, while at large N there is a nonlinear relation. Puff decay time is more sensitive to N than puff rise time is. Qi *et al.* [21] showed that there are linear relations for the interevent interval (including blips and puffs) and the first event latency against the inverse of N. However, nonlinearity is found for the interpuff interval and the first puff latency against the inverse of N. Both puff frequency and blip frequency increase with increasing $[IP_3]$.

Although the effects of $[IP_3]$, cluster size, and Ca^{2+} buffers on puffs have been well studied, little is known about how

*Corresponding address: Department of Physics, Xiamen University, Xiamen, Fujian 361005, China; jianweishuai@xmu.edu.cn

the cytosolic $[Ca^{2+}]_{Basal}$ modulates the puff dynamics. In this paper, we propose an improved two-$[Ca^{2+}]$-level model [21,23,24] to discuss the puff behaviors with the change of N and $[Ca^{2+}]_{Basal}$. An interesting result in our simulation is that, although the increasing $[Ca^{2+}]_{Basal}$ trivially increases the puff frequency and lifetime, the maximal open-channel number and the puff amplitude decrease with the increasing $[Ca^{2+}]_{Basal}$. We show that the underlying dynamics is partly related to the suppressing effect of Ca^{2+} blips on puffs by inhibiting channels to prevent recovery during interpuff intervals. With the increasing $[Ca^{2+}]_{Basal}$, more blips occur to inhibit more channels, leaving fewer channels available for puff events.

II. STOCHASTIC PUFF MODEL

In the paper, we consider a point-source puff model consisting of a stochastic description for IP_3R channels and a deterministic scheme for $[Ca^{2+}]$. The IP_3R channels are discussed with the modified DYK model [25], consisting of four identical independent subunits. Each subunit comprises three sites: an IP_3 binding site (i), an activating Ca^{2+} binding site (j), and an inhibiting Ca^{2+} binding site (k). Each site has two states: binding (1) or unbinding (0). Thus each subunit has eight different states (ijk) as shown in Fig. 1(a). Only the state (110) with both IP_3 and activating Ca^{2+} bound is the active state [the red one in Fig. 1(a)]. The IP_3R channel is open if at least three of the four subunits are in the active state.

As plotted in Fig. 1(a), we classify the eight states of subunits into three groups: the active state (110) which is directly related to the channel open, the three closed states which can become active upon the fast binding of IP_3 and/or Ca^{2+} [the green ones in Fig. 1(a)], and the four inhibited states which have Ca^{2+} bound on the inhibitory binding sites [the yellow ones in Fig. 1(a)]. Once the subunit falls into inhibited states, it will typically remain inhibited for a relatively long time. With the given parameters to fit the experimental data [25,26], the channel open probability against $[Ca^{2+}]$ at different $[IP_3]$ is plotted in Fig. 1(b).

Suppose there are N channels in the cluster. In the model, two different calcium concentrations are proposed for the open and closed channels, respectively [23,24]. It has been shown that the cytosolic $[Ca^{2+}]$ is around 150–220 μM at the surface of an open channel when suggesting $[Ca^{2+}] = 600\,\mu M$ in ER [28]. Thus we simply consider a constant $[Ca^{2+}]_{Open} = 200\,\mu M$ on the open channel in the model.

A dynamical concentration $[Ca^{2+}]_{Close}$ is set for the closed channels, which is actually the domain Ca^{2+} concentration within the channel cluster. $[Ca^{2+}]_{Close}$ was originally suggested to be determined only by the open-channel number [23,24]. Later it was proposed that $[Ca^{2+}]_{Close}$ could be determined not only by the open-channel number, but also by the dye buffer and the sarcoplasmic or endoplasmic reticulum Ca^{2+}-ATPase (SERCA) pump [19]. In our model, besides the exogenous dye buffer, we also consider the effect of the endogenous buffer on $[Ca^{2+}]_{Close}$. As a result, we have

$$\frac{d[Ca^{2+}]_{Close}}{dt} = J_{Cluster} + J_{Leak} - J_{En} - J_{Ex} - J_{Pump}, \quad (1)$$

in which $J_{Cluster}$ denotes the flux of Ca^{2+} from the ER into the cytosol through the open IP_3Rs in the cluster; J_{En} and J_{Ex} represent the effects of the endogenous and exogenous buffers, respectively; and J_{Pump} denotes the effect of the SERCA pump.

The flux $J_{Cluster}$ is given by

$$J_{Cluster} = \gamma([Ca^{2+}]_{Basal} - [Ca^{2+}]_{Close} + N_{Open}\Delta J). \quad (2)$$

Here, γ is the decay rate for the domain collapse, describing the diffusing process of free calcium into the cytosolic space. N_{Open} is the number of the open IP_3Rs and ΔJ is the mean $[Ca^{2+}]$ increment contributed by an open channel to the domain calcium in the cluster.

It is well known that buffers can strongly affect $[Ca^{2+}]_{Close}$. In our model, we consider an endogenous buffer and an exogenous buffer in the cytosol [29]. The equations for buffer dynamics are given in the following:

$$J_{En} = \alpha_{En}([T]_{En} - [Ca^{2+}]_{En})[Ca^{2+}]_{Close} - \beta_{En}[Ca^{2+}]_{En}, \quad (3)$$

$$J_{Ex} = \alpha_{Ex}([T]_{Ex} - [Ca^{2+}]_{Ex})[Ca^{2+}]_{Close} - \beta_{Ex}[Ca^{2+}]_{Ex}, \quad (4)$$

where $[T]_{En}$ and $[T]_{Ex}$ represent the total concentrations of endogenous and exogenous buffers; $[Ca^{2+}]_{En}$ and $[Ca^{2+}]_{Ex}$ denote the concentrations of buffers bound by Ca^{2+}; α_i and β_i denote the on and off rates, respectively.

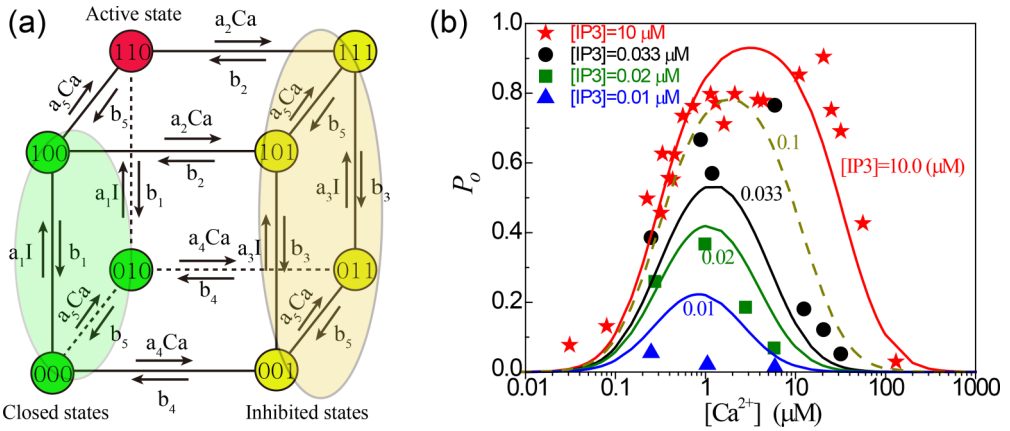

FIG. 1. (a) The schematic diagram of the DYK model for a subunit of the IP_3R channel. Ca and I represent $[Ca^{2+}]$ and $[IP_3]$, respectively. a_i and b_i denote the on and off rates given in Table I. (b) The open probability curve for the DYK model in different cytosolic $[Ca^{2+}]$ and $[IP_3]$. Symbols are experimental data from Refs. [26,27].

TABLE I. Parameter values.

Parameter	Symbol	Value	Unit
IP_3 binding	a_1	1000	$(\mu M\ s)^{-1}$
	a_3	500	$(\mu M\ s)^{-1}$
	b_1	5	s^{-1}
	b_3	100	s^{-1}
Activating Ca^{2+}	a_5	100	$(\mu M\ s)^{-1}$
	b_5	20	s^{-1}
Inhibiting Ca^{2+}	a_2	0.1	$(\mu M\ s)^{-1}$
	a_4	0.1	$(\mu M\ s)^{-1}$
	b_2	5	s^{-1}
	b_4	0.125	s^{-1}
IP_3 concentration	IP_3	0.1	μM
On rates of buffers	α_{En}	150	$(\mu M\ s)^{-1}$
	α_{Ex}	50	$(\mu M\ s)^{-1}$
Dissociation constants of buffers $K_i = k_i^-/k_i^+$	K_{En}	2	μM
	K_{Ex}	2	μM
Total concentration of buffers	T_{En}	40	μM
	T_{Ex}	80	μM
Pump dissociation coefficient	k_{pump}	0.2	μM
Pump flux coefficient	V_{pump}	50	$(\mu M\ s)^{-1}$
Mean $[Ca^{2+}]$ increment	ΔJ	0.6	μM
Decay rate	γ	5000	s^{-1}

The term J_{Pump} denotes the SERCA pump to drive Ca^{2+} ions from the cytosol into the ER in order to keep the high $[Ca^{2+}]$ in the ER [30], which is given by

$$J_{Pump} = V_{Pump}\frac{[Ca^{2+}]^2_{Close}}{[Ca^{2+}]^2_{Close} + k^2_{Pump}}, \quad (5)$$

where V_{Pump} is the maximal calcium uptake, and k_{Pump} is the activation constant for the pump. In the model, we consider a constant leakage J_{Leak} from the ER, which is necessary for establishing a stable resting cytosolic $[Ca^{2+}]_{Basal}$ [30]. As a result, J_{Leak} is a function of $[Ca^{2+}]_{Basal}$.

The values of the parameters are cited from other Ca^{2+} models [16,21,29], which are given in Table I. It has been found that the majority of puff sites are involved in four to six channels in individual clusters in human neuroblastoma SH-SY5Y cells, but some clusters contain ten or more functional channels and some may only have two or three channels [10,13]. In our simulation, we consider two to ten channels in the cluster.

At low $[IP_3]$, most open events in the given cluster are likely to be blips because many channel subunits are IP_3 unbound. However, for high $[IP_3]$, many channels are IP_3 bound and a randomly open channel can easily trigger the other channels to open to generate puffs. As shown in Fig. 1(b), $[IP_3] = 0.1\ \mu M$ is high enough to keep most of the channels IP_3 bound.

III. SIMULATION RESULTS

A. Stochastic Ca^{2+} puffs

In our simulation we run it for 300 s each time to obtain the evolution of N_{Open} and $[Ca^{2+}]_{Close}$. As an example, we plot the traces of N_{Open} and $[Ca^{2+}]_{Close}$ at $N = 4$ in Fig. 2. According to the trace of N_{Open}, we can easily distinguish blips ($N_{Open} = 1$ only) from puffs. To analyze the properties of puffs statistically, we first define some statistical features based on the evolution of N_{Open} and $[Ca^{2+}]_{Close}$. The start of a puff is defined when N_{Open} becomes larger than zero. Because the recovery of $[Ca^{2+}]_{Close}$ from the peak to the resting state is a slow process when the channels are closed, we consider the end of a puff to be the time when $[Ca^{2+}]_{Close}$ decreases back to the concentration that is larger than 20% of $[Ca^{2+}]_{Basal}$. The puff frequency is the inverse of the mean interpuff interval after ignoring all blip events. The puff lifetime is defined as the mean width between two half maxima of $[Ca^{2+}]_{Close}$ at the rising and termination processes of the puffs. The puff amplitude is the average of the maximal $[Ca^{2+}]_{Close}$ of puffs. The average of the maximal open-channel numbers during puffs is also calculated.

First of all, we show that the model with the parameters given in Table I can reproduce the experimental data [14]. In Fig. 2(c), the experimental result of puff frequency as

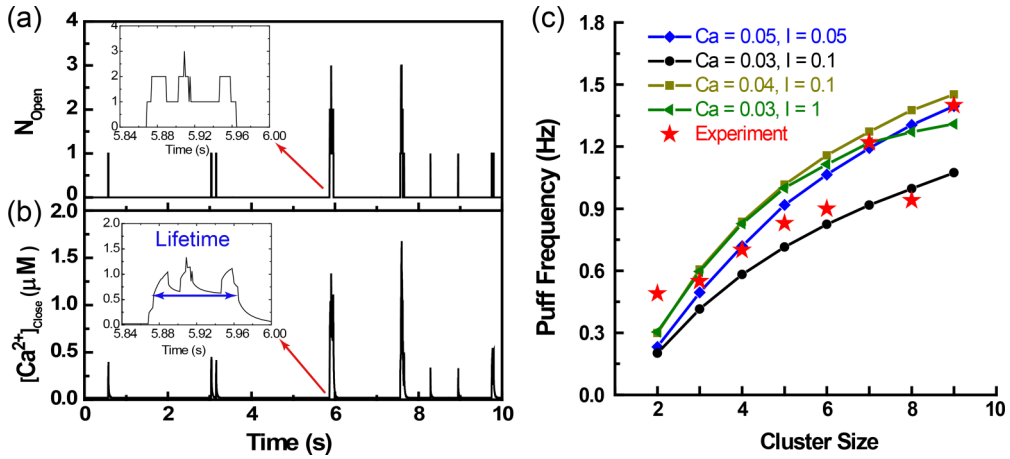

FIG. 2. An example of the simulation result of the model with (a) the evolution of N_{Open} and (b) $[Ca^{2+}]_{Close}$ at $N = 4$. The inner figures are the amplifying puff for N_{Open} and $[Ca^{2+}]_{Close}$. (c) The comparison between experiment and model results for puff frequency against cluster size N. The red stars are experimental data [13]. The solid lines with symbols are obtained with the model at different $[Ca^{2+}]_{Basal}$ and $[IP_3]$.

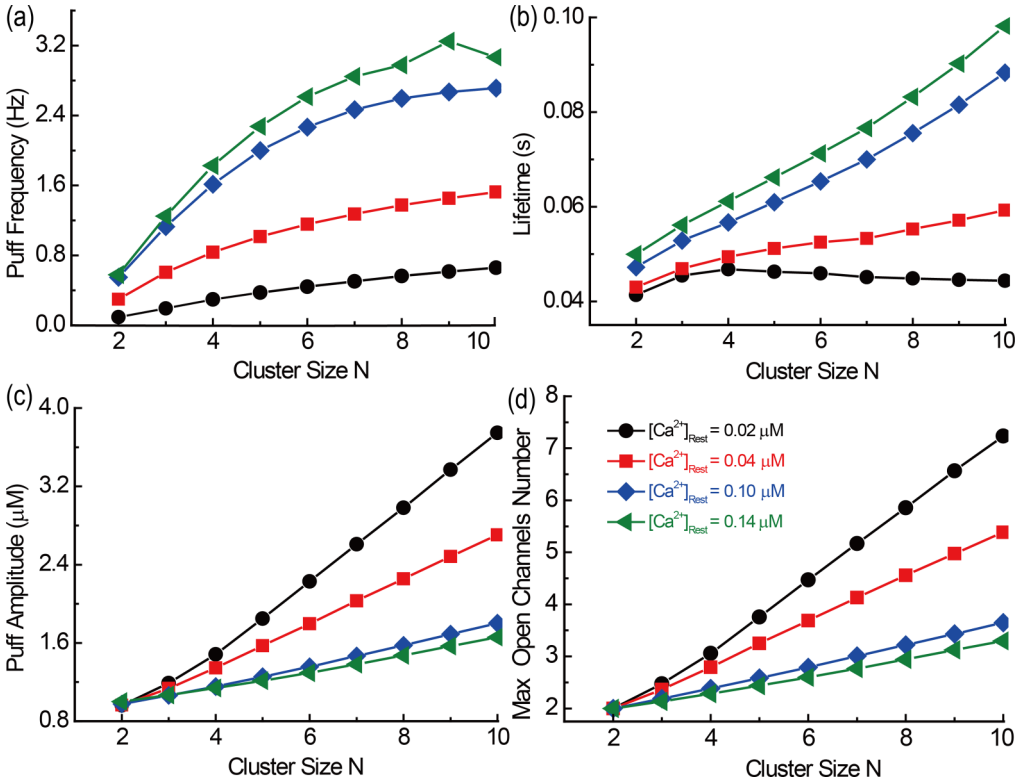

FIG. 3. (a) The puff frequency, (b) puff lifetime, (c) puff amplitude, and (d) the maximal open-channel number against cluster size N at $[Ca^{2+}]_{Basal} = 0.02\,\mu M$ (circles), $0.04\,\mu M$ (squares), $0.10\,\mu M$ (rhombus), and $0.14\,\mu M$ (triangles).

a function of cluster size N is plotted with filled stars. In experiment, all the puffs are generated with strong photolysis flashes (>60 ms) to produce high $[IP_3]$ [14]. It has been suggested that the biological $[Ca^{2+}]_{Basal}$ is typically several tens of nM. Thus, in order to simulate the experimental conditions in our model, we set $[Ca^{2+}]_{Basal} = 0.03$, 0.04, and $0.05\,\mu M$ with $[IP_3] = 0.05$, 0.1, and $1.0\,\mu M$. Figure 2(c) indicates that the puff frequency obtained in our model can well reproduce the experimental data observed in human neuroblastoma SH-SY5Y cells [14].

B. Effects of cluster size on puffs

Now we discuss the puff behaviors as a function of N at different $[Ca^{2+}]_{Basal}$. Figure 3(a) indicates that the puff frequency increases with the increasing N. This is because increasing N means more channels are available not only to be the first open channel, but also to be the channels triggered by the first open channel to produce a puff.

Figure 3(b) shows a plot of the puff lifetime against N. At small $[Ca^{2+}]_{Basal} = 0.02\,\mu M$, the puff lifetime almost stays unchanged with the change of N, while it has a large increase with N at high $[Ca^{2+}]_{Basal}$.

Figures 3(c) and 3(d) show the change of the puff amplitude and the maximal open-channel number of puffs against N, both giving an almost linear relationship. In fact, the puff amplitude is typically determined by the maximal open-channel number during puffs, resulting in a similar relationship against N.

These simulation results that the puff frequency, lifetime, and amplitude, as well as the maximal open-channel number of puffs all monotonically increase with increasing N are consistent with the experimental observations [13–15].

C. Effects of basal $[Ca^{2+}]$ on puffs

Because little is known experimentally and theoretically on how $[Ca^{2+}]_{Basal}$ affects the puff dynamic, in our simulation we discuss in detail the puff behaviors with varying $[Ca^{2+}]_{Basal}$ from 0.02 to $0.2\,\mu M$.

As shown in Fig. 1(b), the open probability of a channel at static equilibrium state increases with the increasing static $[Ca^{2+}]$ at small $[Ca^{2+}]\,(< 1\,\mu M)$ for $[IP_3] = 0.1\,\mu M$. Thus one may expect that, even in the situation with kinetic $[Ca^{2+}]$, the increasing $[Ca^{2+}]_{Basal}$ will provide more active channels, and so the puff frequency, lifetime, and amplitude, as well as the maximal open-channel number of puffs, should monotonically increase also.

As expected, the puff frequency and lifetime both keep rising against $[Ca^{2+}]_{Basal}$ as shown in Figs. 4(a) and 4(b). But surprisingly, there are decreasing relationships for both puff amplitude and the maximal open-channel number responding to increasing $[Ca^{2+}]_{Basal}$, as plotted in Figs. 4(c) and 4(d).

Such decreasing behaviors are unexpected, which indicates that, besides the positive effect of CICR at low Ca^{2+} concentration and the inhibition effect at high Ca^{2+} concentration, there is another suppressing mechanism involved in puff dynamics. Rather than making more channels available for puffs, the increasing $[Ca^{2+}]_{Basal}$ actually induces fewer available channels for puff events, causing decreasing puff amplitude and maximal open-channel number.

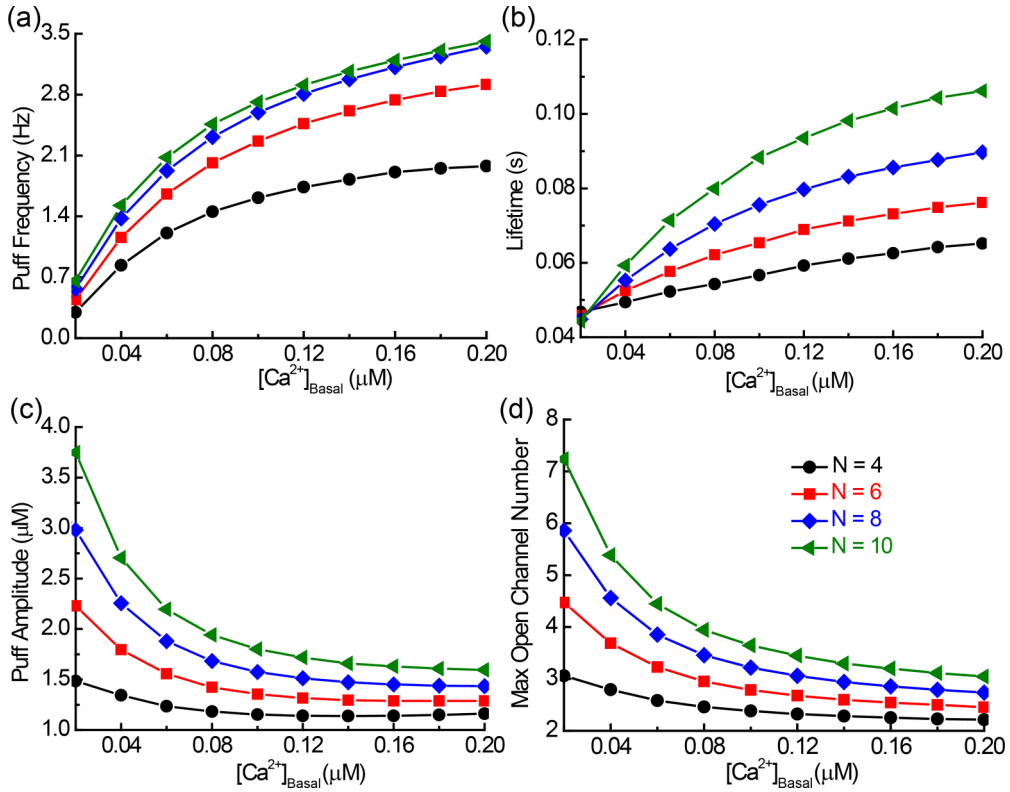

FIG. 4. (a) Puff frequency, (b) puff lifetime, (c) puff amplitude, and (d) the maximum open-channel number against $[Ca^{2+}]_{Basal}$ at $N = 4$ (circles), 6 (squares), 8 (rhombus), and 10 (triangles).

D. Behaviors of probabilities for subunit states

In order to reveal the additional suppressing effect on puff amplitudes with increasing $[Ca^{2+}]_{Basal}$, we discuss the behavior of the subunit states of channels modulated by $[Ca^{2+}]_{Basal}$. Figure 5(a) presents the probabilities of eight states as a function of $[Ca^{2+}]_{Basal}$ at $[IP_3] = 0.1\,\mu M$ and $N = 8$. We can see that the subunits mainly stay in the four states: the active state of (110), the closed state of (100), and the inhibited states of (011) and (111). With the increasing $[Ca^{2+}]_{Basal}$, the probabilities at these four states undergo substantial variation. At low $[Ca^{2+}]_{Basal}$, most subunits stay in the closed state of (100). With the increasing $[Ca^{2+}]_{Basal}$, the probability of the closed state (100) decreases greatly, and the probability of the active state (110) increases due to active Ca^{2+} binding to the (100) state. Meanwhile, the inhibited states of (011) and (111) keep increasing with the increasing $[Ca^{2+}]_{Basal}$.

Figure 5(b) replots the probabilities against $[Ca^{2+}]_{Basal}$ for subunits in the active state, inhibited state, and closed state, i.e., P_{Active}, $P_{Inhibited}$, and P_{Closed}. Figure 5(b) shows that more subunits are in inhibited states at higher $[Ca^{2+}]_{Basal}$, indicating that fewer channels are available for puff events, resulting in the lower puff amplitude.

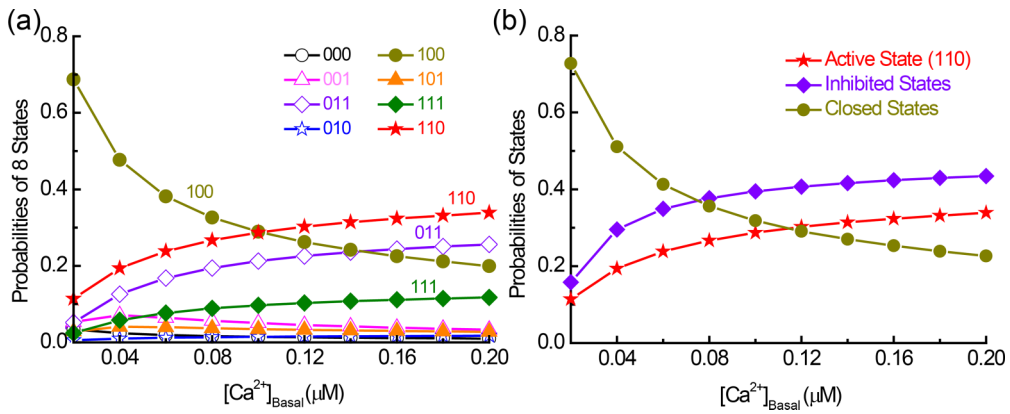

FIG. 5. (a) The probabilities at the eight states and (b) the probabilities of subunits in active state (stars), inhibited states (rhombus), and closed states (circles) against $[Ca^{2+}]_{Basal}$ at $N = 8$.

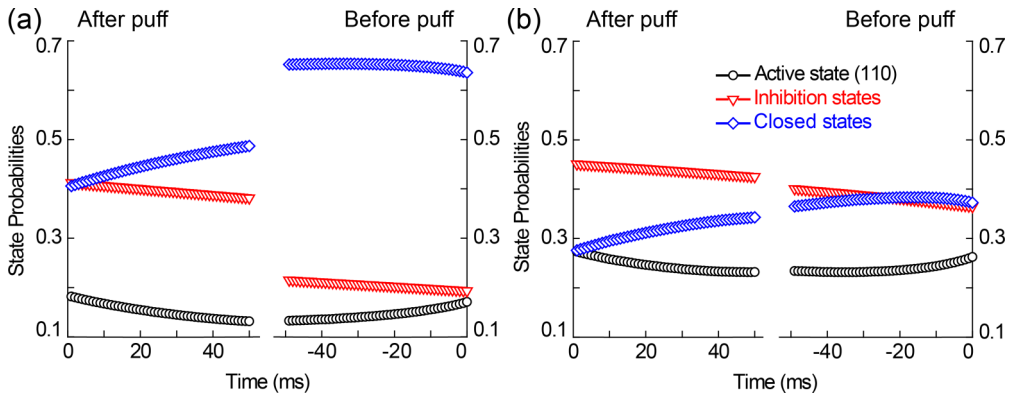

FIG. 6. The evolution of probabilities P_{Active}, $P_{\text{Inhibited}}$, and P_{Closed} for 50 ms right after the termination of puffs and right before the beginning of puffs at $[Ca^{2+}]_{\text{Basal}} = 0.04\,\mu M$ (a), and at $[Ca^{2+}]_{\text{Basal}} = 0.14\,\mu M$ (b) with $N = 8$. The circles denote the active state, triangles the inhibited states, and rhombus the closed states.

In Fig. 5, the probabilities are calculated for all subunits as averages for a long time with many puffs and interpuff intervals. Note that the puff amplitude is actually determined by the available channels before the puff. Thus we focus our investigation more on the subunits during the interpuff intervals.

Figure 6 calculates the evolution of probabilities P_{Active}, $P_{\text{Inhibited}}$, and P_{Closed} right after puffs for 50 ms and right before puffs for 50 ms. As shown in Fig. 6(a) at low $[Ca^{2+}]_{\text{Basal}} = 0.04\,\mu M$, after the termination of puffs most subunits stay in the closed states ($P_{\text{Closed}} \sim 0.4$) and the inhibited states ($P_{\text{Inhibited}} \sim 0.4$). During the recovery, the inhibited subunits keep decreasing, while the closed subunits keep increasing. Before initiating a puff, $P_{\text{Active}} + P_{\text{Closed}}$ increases to 80% with $P_{\text{Inhibited}}$ decreasing to 20%, making most of the subunits available for puffs.

As a comparison, at high $[Ca^{2+}]_{\text{Basal}} = 0.14\,\mu M$ shown in Fig. 6(b), $P_{\text{Inhibited}}$ is about 0.45 right after a puff with $P_{\text{Active}} + P_{\text{Closed}}$ around 0.55. During the recovery, the inhibited subunits decrease slowly. As a result, right before a puff, $P_{\text{Inhibited}}$ is still around 0.36, leaving only 64% of the subunits available for puff events. Figure 6 clearly shows that there is an inhibition process occurring in interpuff intervals, causing the slow recovery for subunits from inhibited states to noninhibited states at high $[Ca^{2+}]_{\text{Basal}}$.

E. The detailed puff trajectories

Now we investigate in detail the recovery process during the interpuff interval by discussing the channel gating trajectories with two examples. Figure 7 plots the trajectories of N_{Open}, $[Ca^{2+}]_{\text{Close}}$, P_{Active}, P_{Closed}, and $P_{\text{Inhibited}}$ at $N = 8$ with $[Ca^{2+}]_{\text{Basal}} = 0.04$ and $0.14\,\mu M$. For both examples, we can observe the following similar processes during puff periods: At the rise period of puffs (red regions in Fig. 7), P_{Active} increases and P_{Closed} decreases to 0 with $P_{\text{Inhibited}}$ staying almost unchanged, indicating a major transition from closed states to active state. Then at the termination period of the puff (yellow regions in Fig. 7), P_{Active} decreases and $P_{\text{Inhibited}}$ increases with P_{Closed} staying around 0, showing a major transition from active state to inhibited states.

Right after the puff termination (green regions in Fig. 7), both examples still present a quite similar recovery process where P_{Active} continually decreases and P_{Closed} increases with $P_{\text{Inhibited}}$ staying almost constant, giving a major transition from active state to closed states.

However, different recovery evolutions are then observed for the two examples. At $[Ca^{2+}]_{\text{Basal}} = 0.04\,\mu M$, P_{Active} stays almost constant, P_{Closed} increases, and $P_{\text{Inhibited}}$ decreases during recovery, indicating a recovery transition from inhibited states to closed states. Differently, at $[Ca^{2+}]_{\text{Basal}} = 0.14\,\mu M$, P_{Active} presents a large fluctuation with P_{Closed} showing a compensating fluctuation, while $P_{\text{Inhibited}}$ typically decreases with P_{Closed} giving a compensating increase. Importantly, the decrease of $P_{\text{Inhibited}}$ is slower at $[Ca^{2+}]_{\text{Basal}} = 0.14\,\mu M$ than at $0.04\,\mu M$.

One obvious reason for the more inhibited channels found right before puffs with higher $[Ca^{2+}]_{\text{Basal}}$ is that the recovery time, i.e., the interpuff interval, is shorter at $[Ca^{2+}]_{\text{Basal}} = 0.14\,\mu M$ than at $0.04\,\mu M$. However, the comparison of $P_{\text{Inhibited}}$ in Fig. 7 indicates that there is another mechanism to cause more channels to be inhibited at high $[Ca^{2+}]_{\text{Basal}}$.

At $[Ca^{2+}]_{\text{Basal}} = 0.14\,\mu M$, more blips are observed in the interpuff interval, as marked by arrows in Fig. 7(f). The occurrence of individual blips not only generates a large fluctuation on P_{Active} during the recovery process, but also induces a small stepped increase of $P_{\text{Inhibited}}$ after the blip, as marked by arrows in Fig. 7(j). As a result, the Ca^{2+} blips present a suppressing effect on puff amplitude by inhibiting channels to prevent their recovery during interpuff intervals.

F. Suppressing effect of Ca^{2+} blips on puff amplitudes

The above discussion indicates an inhibition effect of Ca^{2+} blips on puff dynamics. During the recovery interval of two successive puffs, the stochastic blips occur. After a blip event with only one channel open, at least one subunit has to become inhibited in that channel. Thus the recovery process is prevented by each blip with at least one subunit becoming inhibited.

Figure 8 shows the blip frequency as a function of $[Ca^{2+}]_{\text{Basal}}$ in different N. The increasing $[Ca^{2+}]_{\text{Basal}}$ does not only increase the puff frequency [Fig. 4(a)], but also increases

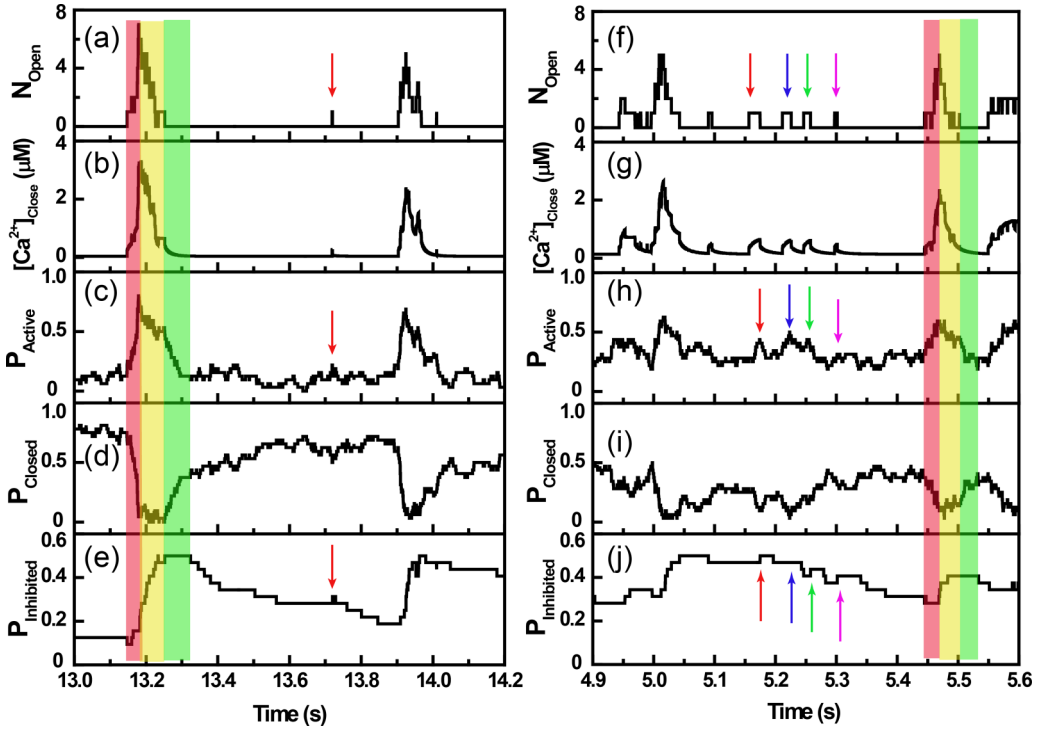

FIG. 7. The detailed traces with $[Ca^{2+}]_{Basal} = 0.04\,\mu M$ (left) and $0.14\,\mu M$ (right) at $N = 8$ in the cluster. The traces are for the number of the open channels (a,f), the domain $[Ca^{2+}]_{Close}$ (b,g), and the probabilities of P_{Active} (c,h), P_{Closed} (d,i), and $P_{Inhibited}$ (e,j).

the blip frequency. More blips produce more inhibited channels to prevent the recovery of channels, leaving fewer channels available for successive puffs. As a result, the maximal open-channel number and the puff amplitude go down with the increasing $[Ca^{2+}]_{Basal}$, as observed in Fig. 4.

IV. DISCUSSION

Ca^{2+} puffs are the elementary Ca^{2+} signals and arise from the opening of several IP_3R channels in a cluster located in the ER membrane. A puff means that more than one channel is open during a release event, while the occurrence of a blip just means that there is only one channel open during the release event. A randomly open channel either can trigger more nearby channels open to generate a puff or fail to trigger any more channels open to present a blip only.

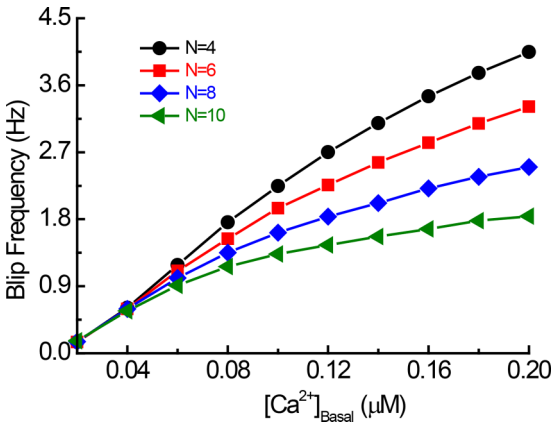

FIG. 8. The blip frequency against $[Ca^{2+}]_{Basal}$ in $N = 4$ (circles), 6 (squares), 8 (rhombus), 10 (triangles).

In this paper, we propose an improved hybrid model with a stochastic dynamics for IP_3R channels and a deterministic dynamics of two-level $[Ca^{2+}]$ for the open and closed channels. A dynamical $[Ca^{2+}]_{Close}$ for closed channels is considered by accounting the effects of the exogenous dye buffer, the endogenous buffer, and the SERCA pump in detail. The process of diffusing free Ca^{2+} into the cytosolic space is implicitly implemented into the point-source model by introducing a decay rate on the Ca^{2+} flux $J_{Cluster}$. In the model we assume that the channel flux is proportional to N_{Open} in Eq. (2). Note that this linear relationship is only applicable in the case of small channel number and large distance among channels [23,31], which is the situation we are dealing with here. Our model is built up for human neuroblastoma SH-SY5Y cells. As shown in the experiment, the majority of puff sites are involved in four to six channels [10,13] with the spatial distance larger than 100 nm between functional IP_3Rs in individual clusters in SH-SY5Y cells [32].

Because little is known about the modulation of $[Ca^{2+}]_{Basal}$ on puff behaviors, we aim to investigate how the puff dynamics would be affected by $[Ca^{2+}]_{Basal}$, as well as N. Consistent with the experimental observations [13–15], our simulations show that monotonically increasing behavior with increasing N can be observed for puff frequency, lifetime, amplitude, and the maximal open-channel number of puffs.

For $[Ca^{2+}]_{Basal}$, its increase trivially causes the increase of puff frequency and lifetime, but unexpectedly generates the reduction of puff amplitude and the maximal open-channel number. We show that the underlying dynamics is related to the increase of both puff and blip frequencies. On one hand,

the higher puff frequency means a shorter recovery time; on the other hand, more blips directly cause more inhibited channels. Both factors actually cause fewer channels to be available for puffs.

During a puff, the channel subunits are mainly self-inhibited [17,23]. In other words, the high Ca^{2+} concentration released from the open channel can inhibit the open channel itself. For the closed channels, as shown in Figs. 3(c) and 4(c), the domain $[Ca^{2+}]_{Close}$ generated by the nearby open channels can become larger than 1 μM, which is also high enough to inhibit the closed channels. These two inhibition processes determine the termination of puffs.

However, one may think it should be an ideal recovery period between two successive puffs, so that those inhibited channel subunits will become uninhibited one by one, gradually. Nevertheless, because of the occurrence of blips, the interpuff interval is not an ideal recovery process. After a blip event, at least one subunit of that open channel has to become inhibited. In other words, the recovery process is prevented by each blip with at least one subunit becoming inhibited. Thus we suggest that there is a suppressing effect of blips on puff amplitudes by inhibiting channels to prevent the recovery process. With the increasing $[Ca^{2+}]_{Close}$, such an inhibition effect becomes stronger because of more blips generated.

It has been an interesting question for a long time how local stochastic Ca^{2+} releases generate global cellular Ca^{2+} waves [20,33–35]. Recent experiment and simulation studies indicate that global repetitive Ca^{2+} waves with long time scales are an emergent property of the stochastic dynamics of the whole cluster array [20,34,35], rather than a merely synchronizing oscillation of IP_3R clusters on the same time scale [33]. As shown in experiment, during the long interwave period increasing puffs will generate the slow accumulation of $[Ca^{2+}]_{Basal}$ [11]. The accumulated $[Ca^{2+}]_{Basal}$ will furthermore increase the puff frequency in turn. Thus there is a positive feedback between $[Ca^{2+}]_{Basal}$ and puff frequency for global Ca^{2+} wave initiation. However, our study here indicates that there is a negative feedback between $[Ca^{2+}]_{Basal}$ and puff amplitude because of the inhibition effect of blips on channels, which might be a mechanism of generation of Ca^{2+} waves with long time scale.

The blips were previously regarded as the failure events for puff generation and could hardly perform any biological functions. Recently, Qi *et al.* [21] suggested that the blips with large release frequency can contribute to increased $[Ca^{2+}]_{Basal}$ and so possibly participate in the initiation of Ca^{2+} waves, especially in small cells with small clusters. In this paper, an interesting inhibition effect is predicted for blips on puff dynamics, which would gain greatly in importance if such experiments of basal calcium effect can be performed. This study shows that the blips may play some nontrivial roles in generating global Ca^{2+} waves through modulating puff dynamics. Thus the blip dynamics may be biologically relevant for Ca^{2+} signaling.

ACKNOWLEDGMENTS

This work was supported by the China National Funds for Distinguished Young Scholars under Grant No. 11125419, the National Natural Science Foundation of China under Grants No. 11504214 and No. 31370830, and the Fujian Province Funds for Leading Scientist in Universities.

[1] M. J. Berridge, P. Lipp, and M. D. Bootman, Nat. Rev. Mol. Cell Biol. **1**, 11 (2000).
[2] M. J. Berridge, M. D. Bootman, and H. L. Roderick, Nat. Rev. Mol. Cell Biol. **4**, 517 (2003).
[3] J. T. Lock, K. L. Ellefsen, B. Settle, I. Parker, and I. F. Smith, J. Visualized Exp. **97**, e52516 (2015).
[4] S. Tang, H.-C. Wong, Z.-M. Wang, Y. Huang, J. Zou, Y. Zhuo, A. Pennati, G. Gadda, O. Delbono, and J. J. Yang, Proc. Natl. Acad. Sci. USA **108**, 16265 (2011).
[5] S. De la Fuente, R. I. Fonteriz, M. Montero, and J. Alvarez, Cell Calcium **54**, 37 (2013).
[6] I. Parker and I. Ivorra, Proc. Natl. Acad. Sci. USA **87**, 260 (1990).
[7] I. Bezprozvanny, J. Watras, and B. Ehrlich, Nature **351**, 751 (1991).
[8] M. J. Berridge, J. Physiol. **499**, 291 (1997).
[9] I. Parker, J. Choi, and Y. Yao, Cell Calcium **20**, 105 (1996).
[10] I. F. Smith and I. Parker, Proc. Natl. Acad. Sci. USA **106**, 6404 (2009).
[11] J. S. Marchant and I. Parker, EMBO J. **20**, 65 (2001).
[12] N. Callamaras, J. S. Marchant, X. P. Sun, and I. Parker, J. Physiol. **509**, 81 (1998).
[13] G. D. Dickinson, D. Swaminathan, and I. Parker, Biophys. J. **102**, 1826 (2012).
[14] G. D. Dickinson and I. Parker, Biophys. J. **105**, 2474 (2013).
[15] S. M. Wiltgen, G. D. Dickinson, D. Swaminathan, and I. Parker, Cell Calcium **56**, 157 (2014).
[16] D. Swaminathan, G. Ullah, and P. Jung, Chaos **19**, 037109 (2009).
[17] G. Ullah, I. Parker, D.-O. D. Mak, and J. E. Pearson, Cell Calcium **52**, 152 (2012).
[18] P. Cao, G. Donovan, M. Falcke, and J. Sneyd, Biophys. J. **105**, 1133 (2013).
[19] S. Swillens, G. Dupont, L. Combettes, and P. Champeil, Proc. Natl. Acad. Sci. USA **96**, 13750 (1999).
[20] M. Rückl, I. Parker, J. S. Marchant, C. Nagaiah, W. F. Johenning, and S. Rüdiger, PLoS Comput. Biol. **11**, e1003965 (2015).
[21] H. Qi, Y. Huang, S. Rüdiger, and J. Shuai, Biophys. J. **106**, 2353 (2014).
[22] S. Rüdiger, C. Nagaiah, G. Warnecke, and J. Shuai, Biophys. J. **99**, 3 (2010).
[23] S. Rüdiger, J. Shuai, and I. Sokolov, Phys. Rev. Lett. **105**, 048103 (2010).
[24] S. Rüdiger, P. Jung, and J.-W. Shuai, PLoS Comput. Biol. **8**, e1002485 (2012).
[25] G. W. De Young and J. Keizer, Proc. Natl. Acad. Sci. USA **89**, 9895 (1992).
[26] D.-O. D. Mak and J. K. Foskett, J. Gen. Physiol. **109**, 571 (1997).

[27] D.-O. D. Mak, S. McBride, and J. K. Foskett, Proc. Natl. Acad. Sci. USA **95**, 15821 (1998).
[28] K. Bentele and M. Falcke, Biophys. J. **93**, 2597 (2007).
[29] S. Rüdiger, J. W. Shuai, W. Huisinga, C. Nagaiah, G. Warnecke, I. Parker, and M. Falcke, Biophys. J. **93**, 1847 (2007).
[30] E. Carafoli, Nat. Rev. Mol. Cell Biol. **4**, 326 (2003).
[31] T. Schendel, R. Thul, J. Sneyd, and M. Falcke, Eur. Biophys. J. **41**, 27 (2012).
[32] S. M. Wiltgen, I. F. Smith, and I. Parker, Biophys. J. **99**, 437 (2010).
[33] J. Shuai, Y. Huang, and S. Rüdiger, Phys. Rev. E **81**, 041904 (2010).
[34] K. Thurley, I. F. Smith, S. C. Tovey, C. W. Taylor, I. Parker, and M. Falcke, Biophys. J. **101**, 2638 (2011).
[35] K. Thurley and M. Falcke, Proc. Natl. Acad. Sci. USA **108**, 427 (2011).